Probing Hydrogen Bond Networks in Half-Sandwich Ru(II) Building Blocks by a Combined 1H DQ CRAMPS Solid-State NMR, XRPD, and DFT Approach

INORGANIC CHEMISTRY, 53 (2014), 139-146

DOI: 10.1021/ic401762z

Probing hydrogen bond networks in half-sandwich Ru(II) building-blocks by a combined ^{1}H DQ CRAMPS solid-state NMR, XRPD and DFT approach

Michele R. Chierotti,[a] Roberto Gobetto,[a] Carlo Nervi,[a] Alessia Bacchi,[b] Paolo Pelagatti,[b] Valentina Colombo,[c] Angelo Sironi[c]**

[a]Department of Chemistry and NIS Centre of Excellence, University of Torino, Via P. Giuria 7, 10125 Torino, Italy.

[b]Department of Chemistry, University of Parma, Parco Area Scienze 17/A, 43124 Parma, Italy.

[c]Department of Chemistry, University of Milano, Via Golgi 19, 20133 Milano, Italy.

Keywords. solid-state NMR, ^{1}H double-quantum CRAMPS, periodic calculation, hydrogen bond network, polymorphism, XRPD structure solution, PMLG pulse sequence

Abstract: The hydrogen bond network of three polymorphs (**1α**, **1β** and **1γ)** and one solvate form (**1·H$_2$O**) arising from the hydration-dehydration process of the Ru(II) complex [(*p*-cymene)Ru(κN-INA)Cl$_2$] (INA = isonicotinic acid), has been ascertained by means of 1D and 2D double quantum ^{1}H CRAMPS (Combined Rotation and Multiple Pulses Sequences) and ^{13}C CPMAS solid-state NMR experiments. The resolution improvement provided by homonuclear decoupling pulse sequences with respect to fast MAS experiments has been highlighted. The solid-state structure of **1γ** has been fully characterized by combining X-Ray powder diffraction, solid-state NMR and periodic plane-wave first principles calculations. None of the forms shows the expected supramolecular cyclic dimerization of the carboxylic functions of INA, owing to the presence of chlorine atoms as strong hydrogen bond acceptors. The hydration-dehydration process of the complex has been discussed in terms of structure and hydrogen bond rearrangements.

Introduction.

Non covalent interactions are key features in determining crystal packing differences and, thus, property differences in polymorphic and solvate systems.[1] Among all weak interactions, the hydrogen bond (HB) is the most important because it combines directionality and strength with selectivity, leading to one-, two-, or three-dimensional (1D, 2D or 3D) architectures, or new co-crystals with peculiar properties.[2]

The characterization of different HB-based polymorphs represents an important challenge since it implies the study of weak interactions, which are responsible of the unique properties shown by each polymorph. This allows packing-property correlations to be made and then the design of periodic and organized structures with desired and tunable features. In these studies, X-ray Single Crystal Diffraction (XRSCD) is certainly the best technique which is nevertheless not suitable when dealing with very small crystals (powders). In the latter case, a reliable alternative is ab-initio X-ray Powder Diffraction (XRPD)[3] which can be profitably complemented by Solid-State NMR (SSNMR) and DFT computational methods.[4] Indeed, XRPD provides long range information such as (time and space) averaged symmetry and atomic positions, while SSNMR relies on local (short range) information at each independent site to address the 'size' of the asymmetric unit and the stereochemistry of relevant fragments and tectons (by looking at ^{1}H-^{1}H and ^{1}H-^{13}C proximities).[5] Very fast magic angle spinning (MAS) at 70 kHz or Combined Rotation and Multiple Pulses Sequences (CRAMPS) such as DUMBO, PMLG…,[6] allow the location of hydrogen-bonded proton signals which experience high frequency shifts whose magnitude strongly depends on HB length and strength.[7] On the other hand, by means of ^{1}H 2D double quantum (DQ) MAS or CRAMPS NMR experiments it is possible to obtain additional information on intra- and intermolecular ^{1}H-^{1}H proximities up to~3.0 Å useful for elucidating HB networks. DFT-based periodic calculations applied to the solid state helps in solving structures, elucidating spectroscopic properties and determining

energy differences between polymorphs or even in preventing an incorrect structure determination from powder data.[8]

We have recently characterized the behaviour of a promising building-block for wheel-and-axle systems: the half sandwich Ru(II)-complex [(p-cymene)Ru(κN-INA)Cl_2] (**1**, INA = isonicotinic acid).[9] Wheel-and-axle compounds (WAA) are dumbbell shaped molecules where a linear ditopic ligand bridges two relatively bulky groups.[10] These systems are able to reversibly absorb several volatile organic compounds through heterogeneous solid-gas processes,[11] thus being good candidates for the development of gas sensors or gas-storage devices. In our case, INA was expected to bind Ru through the py-N donor and at the same time to give rise to the cyclic dimerization of the COOH functions thus creating the axle of the WAA system. Although the py-binding to Ru was confirmed, the COOH groups dimerization was prevented by the formation of intermolecular Ru-Cl…HOOC HBs isolating the room temperature stable polymorph **1α** (Scheme 1a). Once exposed to water vapors, **1α** quickly converted into **1·H_2O** (Scheme 1b) that, upon heating, afforded an anhydrous polymorph, **1β** (Scheme 1a), through a transient intermediate, **1γ**. Such hydration-dehydration processes are summarized in Scheme 1c. All the reported phases, but **1γ**, were structurally characterized either by XRSCD (**1α** and **1·H_2O**) or XRPD and SSNMR approach (**1β**).[9]

The number of studies dealing with organometallic polymorphism is certainly limited if compared to the huge amounts of reports on organic polymorphism,[12]possibly because the main field of application of organometallics, i.e. homogeneous catalysis, concerns their solutions.

Here, we report on the isolation of the pure **1γ**polymorph and its XRPD/NMR/DFT structural characterization that was previously hindered by the lack of long standing pure samples. Thermodiffractometry allowed the recognition of pure **1γ** at RT and, later, its structural characterization. The use of ^{1}H MAS and CRAMPS (*w*PMLG5) and ^{1}H 2D DQ

CRAMPS (PMLG5-POSTC7-*w*PMLG5) SSNMR techniques has been fundamental for adding spectroscopic evidences on HB networks in all forms. Periodic plane-wave DFT calculations were actively used to confirm and refine all experimental information. Eventually this synergic coupling of different approaches led to a better understanding of the whole system.

In light of these new results, this paper is also an opportunity to discuss the hydration-dehydration process of the Ru(II) complex in terms of HB, crystal packing rearrangements and polymorph stabilities. For a thorough analysis, forms **1α** and **1·H$_2$O**, whose X-ray structures are available, will be used for comparison together with the analogue Ru(II) complex [(p-cymene)Ru(κN-A4AB)Cl$_2$] (**2**)[13] (A4AB= 4-aminobenzoic acid) (Scheme 1d) and the free ligands INA and A4AB.

Experimental Details.

SSNMR spectroscopy. SSNMR measurements were run on a Bruker AVANCE II 400 instrument operating at 400.23 and 100.65 MHz for ^{1}H and ^{13}C, respectively. ^{13}C and ^{1}H-^{13}C HETCOR spectra were recorded at room temperature at the spinning speed of 12 kHz. Cylindrical 4mm o.d. zirconia rotors with sample volume of 80 μL were employed. For ^{13}C CPMAS experiments, a ramp cross-polarization pulse sequence was used with contact times of 4 ms, a ^{1}H 90° pulse of 3.30 μs, recycle delays of 1.5 s, and 1024 transients. The two pulse phase modulation (TPPM) decoupling scheme was used with a frequency field of 75 kHz. 2D ^{1}H-^{13}C on- and off-resonance HETCOR spectra were measured according to the method of van Rossum et al.[14] with setup previously described.[15] The ^{1}H chemical shift scale in the HETCOR spectra was corrected by a scaling factor of 1/√3 since the ^{1}H chemical-shift dispersion is scaled by a factor of 1/√3 during FSLG decoupling. ^{1}H MAS, ^{1}H CRAMPS and 2D ^{1}H DQ CRAMPS experiments were performed on a 2.5 mm Bruker probe. The ^{1}H MAS spectra were acquired at the spinning speed of 32 kHz with the DEPTH sequence (π/2–π–π)

for the suppression of the probe background signal. ^{1}H CRAMPS spectra were acquired using a windowed-PMLG (*w*PMLG5)[16] pulse sequence of dipolar decoupling at the spinning speed of 12.5 kHz. 2D ^{1}H DQ CRAMPS spectra were acquired at the spinning speed of 12.5 kHz with PMLG5 and *w*PMLG5 pulse sequences for homonuclear dipolar decoupling during t_1 and t_2, respectively. For all samples, ^{1}H 90° pulse lengths of 2.5 μs and recycle delays of 3 s were used. For each of 256 increments of t_1, 80 transients were averaged. The pulse width and the RF power were finely adjusted for best resolution. In t_2, one complex data point was acquired in each acquisition window (2.2 μs). DQ excitation and reconversion was achieved using three elements of POST-C7,[17] corresponding to a recoupling time of 68.58 μs. A 16-step nested phase cycle was used to select $\Delta p=\pm 2$ on the DQ excitation pulses (four steps), and $\Delta p=-1$ on the z-filter 90° pulse (four steps). The States-TPPI method was used to achieve sign discrimination in the F1 dimension. ^{1}H and ^{13}C scales were calibrated with adamantane (^{1}H signal at 1.87 ppm) and glycine (^{13}C methylene signal at 43.86 ppm) as external standards.

X-ray powder diffraction measurements and analysis. All the diffraction data (Cu Kα_{12}, 1.5418 Å) were collected on a θ:θ Bruker AXS D8 Advance vertical scan diffractometer; the generator was operated at 40 kV and 40 mA. The diffractometer was equipped with a Ni filter and a linear Position Sensitive Detector (PSD), with the following optics: primary and secondary Soller slits, 2.3 and 2.5°, respectively; divergence slit, 0.3°; receiving slit, 8 mm. The nominal resolution for the present set-up is 0.08° 2θ (FWHM of the α1 component) for the LaB_6 peak at about 21.3° (2θ). The conditioning chamber for thermodiffractometric experiment, a closed Peltier sample heater, was supplied by Officina Elettrotecnica di Tenno, Italy. The accurate diffraction pattern at RT under nitrogen of the pure **1γ** phase was acquired in the 4-90° 2θ range, with $\Delta 2\theta = 0.02°$ and exposure time 1 s/step. The pattern was indexed using the single value decomposition approach[18] which afforded a monoclinic lattice (P21/a space group, a = 30.986(2), b = 15.3681(9), c = 7.3828(4), β = 95.281(4); Le Bail Rwp 4.39)

later confirmed by the finding, upon exhaustive simulated annealing runs,[19]a good structural hypothesis (Rwp 10.15), which was successfully refined (final Rp, Rwp and RBragg: 4.02, 5.28 and 2.27, respectively).

During simulated annealing, we described the molecule as a single "flexible" rigid body allowing for all necessary rotations. At variance, during refinements, the Ru-(η^6-p-cimene) and the p-carboxyl pyridine groups were treated as independent, "flexible" (both the isopropyl and carboxyl group rotations were allowed) rigid bodies. The chlorine atoms were free to refine but the Ru-Cl and Ru-N bond distances were restrained to 2.44 and 2.12 Å, respectively. "Antibump" conditions were substantial for a correct sampling of the conformational space.[20] The final refinement was done using the DFT optimized structure as 'reference' (see main text and note 32) maintaining only the Ru-Cl and Ru-N restrains.

Peak shapes were described by the fundamental parameters approach.[21] The experimental background was fit by a polynomial description. Systematic errors were modelled with sample-displacement angular shifts corrections. Metal and chlorine atoms were given a refinable, isotropic displacement parameter (BM) while lighter atoms were assigned a common B = BM + 2.0 $Å^2$ value. All computations were performed with TOPAS using scattering factors, corrected for real and imaginary anomalous dispersion terms, taken from its internal library.[22]

Computational details. Periodic lattice calculations were performed by means of Quantum Espresso, version 4.3.2,[23] keeping constant the cell parameters (i.e. no cell optimizations have been performed)and the Ru atom coordinates, which are the most accurate XRPD parameters. Vanderbilt Ultrasoft pseudo-potentials (USPP)[24] including scalar relativistic corrections were used for all atoms (employing those available at the Quantum Espresso web site).[25] The general gradient approximation (GGA) with the Perdew–Burke–Ernzerhof (PBE) functional[26] was used in the calculations. We thoroughly used a cut-off energy of 60 Ry for plane-waves

USPP calculations to ensure convergence. The high cut-off chosen is required by the presence of atoms, like oxygen, for which even the ultrasoft pseudopotential is relatively hard. Note, however, that a lower level of convergence would not affect significantly the conclusions drawn in this work. Due to the large cell size and to their shapes, the irreducible Brillouin zones were sampled with only one (for **1β**) or two k-points (2×1×1 for **1γ**), with the Monkhorst–Pack scheme.[27] Gaussian 09[28] GIAO method has been used to compute NMR chemical shifts of **1γ**. We employed the DFT method with Becke's three parameter hybrid functional[29]and Lee-Yang-Parr's gradient-corrected correlation functional (B3LYP).[30] The Los Alamos double-ζ (LanL2Dz) basis set and effective core potential were used for Ru atoms, and the split-valence 6-31+G(d,p) basis set was applied for all other atoms. The chemical shifts were computed extracting two structures from the optimized **1γ** cell unit: four and three molecules of the first neighbouring shell have been selected around the strong and the weak H···Cl interactions, respectively.The calculated absolute magnetic shielding σ values were converted into ^{1}H chemical shifts δ relative to the absolute magnetic shielding of TMS (σ = 31.6412), computed at the same B3LYP/6-31+G(d,p) level.

Results and Discussion.

Solid-state synthesis of 1γ and reformulation of the qualitative phase diagram. VT-XRPD experiments show that although **1β** can be stabilized at RT by quenching from 90°C to RT, it is only metastable. Indeed, if slowly cooled, it transforms into **1γ**. The **1β→1γ** phase transition occurs at ca. 35 °C, while the backward transformation **1γ→1β** starts above 40 °C. The same experiments performed by keeping the temperature constant just above the onset (80 °C), confirm the crystal-to-crystal nature of the **1·H$_2$O→1γ** and **1γ→1β** transformations (see Fig. S1 in the supporting information). The instability of **1γ** at 80°C and the inherent presence of some phase contamination (heavy in the intermediate at 80 °C but only slight at RT), do not

hamper to confirm that the powder pattern of the intermediate phase **1γ**, reported in Fig 1c, well matches with that obtained by cooling under N_2 (Fig 1e). Thus, the originally proposed qualitative phase diagram (Scheme 1c) must be redrawn as in Scheme 2. The lack of amorphous intermediates during the **1·H$_2$O→1γ** and **1γ→1β** processes and their reversibility indicate their topotactic nature *i.e.* the structures of **1·H$_2$O**, **1γ** and **1β** must have a high degree of similarity.

The characterization of the hydration-dehydration processes has been completed by the *ab-initio* XRPD structural determination of **1γ** taking full advantage of the complementary information granted by SSNMR and computational techniques.

SSNMR data on 1γ. ^{1}H and ^{13}C chemical shifts with assignments for compound **1γ** are reported in Table 1. ^{1}H and ^{13}C assignment has been based on data of **1α** and **1β** previously reported[9] and with the help of the ^{1}H-^{13}C FSLG-HETCOR experiment (see Fig. S2 in the supporting information). However, it was not possible to discriminate and assign the resonances (in particular the ^{1}H ones still quite broad) for the symmetry nonequivalent molecules. The splitting of all ^{13}C resonances in the ^{13}C CPMAS spectrum of **1γ**, shown in Fig. 2a, not observed for **2** (Fig 2b), clearly highlights the presence of two independent molecules in the unit cell (Z'=2; for a thorough comparison ^{13}C spectra of **1α**, **1·H$_2$O** and **1β** are reported in Fig. S3). The chemical shift difference (~4.4 ppm) for the two C6 (COOH) nuclei in **1γ** (167.3 and 162.9 ppm) suggests two different HB arrangements. However, both sites do not seem to form the cyclic dimerization which would result in a high frequency shift similar to that observed in **2**, (C6 at 172.7 ppm, Fig. 2b).The cyclic dimerization is definitely ruled out by the analysis of the DQ correlations in the ^{1}H DQ CRAMPS spectrum, where the presence of DQ signals implies a ^{1}H–^{1}H through-space separation of less than ~3 Å with $\delta_{DQ}=\delta_A+\delta_B$ for $^{1}H^{A}$–$^{1}H^{B}$ proximities (two symmetric signals with respect to the diagonal) or $\delta_{DQ}=2\delta_A$ for

$^1H^A$–$^1H^A$ intermolecular separation (one peak on the diagonal).[31] In the case of compound **2** whose spectrum is reported in Fig. 3, the presence of the COOH cyclic motif (which brings two OH of different molecules closer than 3 Å) leads to a DQ coherence at δ_{DQ}=13.3+13.3=26.6 ppm (diagonal correlation), as expected. On the contrary, in the ^1H DQ CRAMPS spectrum of **1γ**, shown in Fig. 4, the lack of DQ coherences at δ_{DQ}=10.5+10.5=21.0 ppm definitively indicates the absence of COOH dimerization. Other DQ signals involving OH protons are collected in Table 2.

The comparison between ^1H MAS spectra of **1β** and **1γ**, reported in Fig. 5, shows a halving of the **1β** OH signal intensity. This can be attributed either to a reduction of the number of protons involved in the O-H···Cl or to the presence of a very weak HB leading to a OH signal overlapped with that of the aromatic protons. Proton mobility along the HB has been ruled out by recording spectra at different temperatures.

Crystal Structure of 1γ and a short reappraisal of that of 1β. The structure of **1γ** was solved, *ab-initio*, from laboratory XRPD pattern. **1γ** crystallizes in the Monoclinic, $P2_1/a$, space group (No 14, non standard setting of $P2_1/c$) with 2 independent molecules in the asymmetric unit (Z = 8, Z' = 2) and the largest molecular volume, V_M = V/Z, among the three anhydrous polymorphs **1α**, **1γ** and **1β** (421, 437 and 425 $Å^3$, respectively). The molecular structure and labelling scheme of **1γ** are reported in Fig. 6.

XRPD, particularly when using laboratory instruments, affords blurry molecular pictures. Presently, dealing with two molecules in the asymmetric unit (of volume 874 $Å^3$) and 44 independent non-hydrogen atoms, we were forced to use a heavy idealization. In the present case, diffraction possibly affords only the rough shape and location of the two independent molecules but does not shed enough light neither on the metrical details of covalent bonding nor on the topology of intermolecular interactions. Indeed, while we clearly observe one short

O-H···Cl (O1b···Cl2a) contact and unambiguously exclude the presence of any COOH cyclic dimer, we are unable to decide whether the second independent carboxylic group does interact or not with its closest chlorine atom since the O1a···Cl2b distance is rather elongated and strongly dependent from the details of the anti-bumping conditions on the nearby atoms. Thus, periodic lattice DFT calculations were performed on the**1γ** XRPD structure in order to increase the accuracy of XRPD results and to ascertain the intermolecular role of this second carboxylic group, and the structure resubmitted for Rietveld refinements. The iteration method, repeated until self-consistency, leads to a final **1γ**-XRPD model.[32] The structure is characterized by one strong (O···Cl distance of 3.085Å and O-H-Cl angle of 166.2°) and one weak (O···Cl distance of 3.183 Å and O-H-Cl angle of 156.2°) O···Cl interactions. This agrees with the ^{1}H MAS NMR spectra (see above) and with NMR-GIAO DFT calculations data (in this case GIPAW calculation would be prohibitive).[33] Indeed, both suggested that only half of the OH hydrogen atoms are involved in strong O-H···Cl interactions while the others, attributed to a weaker contact, fall overlapped under the signals of aromatic hydrogen atoms in ortho position with respect to the pyridine nitrogen atoms (computed chemical shifts: 12.2 and 9.6 ppm for the strong and weak interaction, respectively). Another optimized structure characterized by only one O···Cl contact had higher energy[34] or did not fit XRPD data. The iterative approach herein adopted allowed to discover, *inter alia*, that the previously reported **1β** structure had a wrong conformation of the p-cymene i-propyl group (see above). We were able to found a better Rwp minimum (6.52 vs. 6.79) in which the i-propyl group has the same conformation found in **1·H$_2$O**. Accordingly, the last sentence of page 4371 of ref 9 must be reconsidered (and Fig. 13b modified) given that the molecules in **1·H$_2$O** and **1β** differ only in the carboxyl rotation (see Supplementary Information). The new **1β** XRPD model was then resubmitted to Quantum Espresso leading to a O···Cl distance of 3.086 Å (OH···Cl distance = 2.106 Å; C-H-Cl angle =

162.6°). This interaction is relatively strong, and fits perfectly with the SSNMR observation of a single strong O-H···Cl HB.

Finally, **1β** and **1γ** polymorphs have very similar absolute energy per molecule. This observation is also in agreement with the overall picture proposed.

HB network analysis. High resolution ^{1}H 1D (Fig 7 together with the corresponding hydrogen bond contacts) and 2D DQ CRAMPS (Fig. 3 and 4, and S4-S8 in the supporting information) SSNMR spectra (**1α**, **1β**, **1γ**, **1·H$_2$O**, and **2**) allowed elucidating the HB networks of all polymorphs and confirm the accuracy of the **1β** and **1γ** structures solved from powder data. All OH proton chemical shifts with main ^{1}H-^{1}H proximities obtained from the 2D spectra are listed in Table 2.

While a resolution improvement is observed for all signals by using the *w*PMLG5 method compare to MAS experiments, we focus our discussion herein on the DQ signals involving hydrogen-bonded protons. X-ray single-crystal structure analysis reveals similar intermolecular hydrogen-bonding arrangements *i.e.* the contact O-H···Cl, for the three polymorphs **1α**, **1β** and **1γ**. This is reflected in similar chemical shift values of the OH resonance at 9.9, 10.1 and 10.5 ppm, respectively. These structures do not show the expected supramolecular cyclic dimerization of the carboxylic functions of INA as confirmed by the lack of diagonal peaks associated to the OH resonance in their ^{1}H DQ CRAMPS spectra (Fig. 4 and Fig. S4-S5). This is in agreement with the good HB-acceptor character of the Cl ligands.[35] For **1β** DQ signals involving the OH protons are at δ_{DQ}=10.1+1.6=11.7 ppm (intermolecular with H15 and H16 - methyl groups of the isopropyl moiety) and δ_{DQ}=10.1+8.5=18.6 ppm (intermolecular with H2 - pyridyl aromatic proton of another molecule), see Fig. S4. In the ^{1}H 2D DQ CRAMPS spectrum of **1γ** we observed proximities between OH and H16 (methyl group of the isopropyl moiety) (δ_{DQ}=10.5+1.7=12.2), OH and

H14 (CH group of the isopropyl moiety) (δ_{DQ}=10.5+3.2=13.7) and between H10 and H5 (pyridyl proton) (δ_{DQ}=10.5+8.9=19.4). The ^{1}H-^{1}H proximities observed in the ^{1}H 2D DQ CRAMPS NMR spectra of **1β** and **1γ** perfectly agree with the structure solved from XRPD and optimized by DFT providing useful parameters for validating the reliability of the structure solved from powder data. In **1α** the OH group results quite far from other hydrogen atoms as confirmed by the presence of only one DQ resonance at δ_{DQ}=9.9+5.0=14.9 attributed to the H10-H11 (aromatic proton) proximity (Fig. S5). **1·H$_2$O** shows two water molecules bridging two carboxylic functions of two different metallorganic entities, giving rise to a $R^4_4(12)$ supramolecular cyclic dimer.[36] Owing to casual overlapping, the location at 4.7 ppm of the proton water signal in the spectrum was possible only through the H10-Hw proximity generating a DQ correlation at δ_{DQ}=8.7+4.7=13.4 (Fig. S6). The other correlation refers to the H10-H16 proximity (δ_{DQ}=8.7+1.4=10.1).

As stated above, the **2** analogue presents the supramolecular cyclic dimerization of the COOH group as highlighted in the ^{1}H DQ CRAMPS spectrum (Fig. 3). A similar diagonal peak indicating the COOH dimerization characterizes also the spectrum of the pure ligand A4AB (see Fig. S7 and Scheme S1 for a sketch of the intermolecular contacts): δ_{DQ}=13.9+13.9=27.8.[37] On the contrary, the pure ligand INA presents O-H···N head-to-tail interactions (see Scheme S2),[38] thus its 2D DQ spectrum (see Fig. S8) does not shows OH diagonal peaks but DQ signals at δ_{DQ}=18.1+8.5=26.6 (OH-H2 and H6 pyridine hydrogen atoms) andδ_{DQ}=8.2+8.2=16.4 (H2-H3 and H5-H6 pyridine hydrogen atoms).

Structural correlation between 1·H$_2$O, **1γ** and **1β.** For comparing the three structures we considered for**1·H$_2$O** and **1β** a super cell of order 2 with the same SG symmetry ($P2_1/a$) of **1γ** and lattice parameters similar to those of **1γ**.

A quick look at Fig. 8, where the content of the three (super)cells is reported and the O-H···Cl interactions are highlighted, clearly shows that the entropy-driven water desorption of **1·H$_2$O** (which implies the rupture of 16 O-H···O and 8 O$_w$-H···Cl interactions per super-cell) determines a topotactic volume shrinkage (from 3677 to 3492 Å^3, which, however, still leaves some residual voids) to **1γ** associated to the formation of 8 new O-H···Cl interactions per cell. Then, a further volume shrinkage (from 3492 to 3389 Å^3) and the reorganisation of 4, out of 8, O-H···Cl interactions per super-cell, leads to **1β**. Actually, Fig 8A is slightly misleading since the projection of the structures down c shades that the **1·H$_2$O→1γ** phase transition implies not only a doubled cell but also a structural shear along ***a**** at the interface of the carboxylic groups as highlighted in Fig. 9. No additional shear was observed in the following **1γ→1β** transition and, as expected, **1γ** is more similar to **1β** than to **1·H$_2$O.**

Conclusion.

In this contribution we demonstrate how high resolution ^{1}H CRAMPS (1D and 2D) SSNMR techniques, XRPD techniques and periodic plane-wave first principles calculations can be combined for providing reliable structures of organometallic microcrystalline samples not suitable for a single crystal X-ray analysis.

XRP thermodiffractometry allows both to follow complex phase transformations and to structural characterize 'uncontaminated' intermediates, thus affording substantial information suitable as starting points for SSNMR analysis and DFT plane wave periodic calculation. On the other hand, SSNMR affords a separate evaluation of the number of crystallographically independent fragments which is highly useful in the XRPD indexing process. Finally, DFT plane wave periodic calculation together with the ^{1}H-^{1}H proximities, obtained by ^{1}H DQ CRAMPS spectra, provide an efficient method for checking the reliability of the solved structure.

Thanks to this integrated multiple approach, which is intrinsically more accurate than the single methodologies, a complete characterization of the [(*p*-cymene)Ru(κN-INA)Cl_2] polymorphic system has been performed. The hydrogen bond networks in all systems have been investigated in term of supramolecular synthons. The phase transformations have been analyzed by thermodiffractometry. Passing from **1·H_2O** to **1γ** and from **1β** to **1γ**, the sequence of continuous shrinkages and gradual formations of O-H···Cl interactions is coherent with the metastable nature of **1γ** at 80°C. However, we were not expecting to retrieve **1γ** on cooling **1β** at RT (under N_2 atmosphere), as we have, later on, found.

The structural correlation between **1·H_2O**, **1γ** and **1β**, which mainly depends from their space group symmetries, lattice metrics and rough molecules locations and orientations within the unit cells, has been recognized. Noteworthy, this result greatly improves the level of confidence of our *ab-initio* XRPD structure solution and, possibly, addresses the most probable mechanism of **1·H_2O**, **1γ** and **1β** polymorphic transformation.

In view of the current interest on the anticancer activity of half-sandwich Ru(II) complexes,[39] the knowledge of the polymorph-dependent stability and hygroscopicity for molecules belonging to this class of compounds (compare the relative affinities of the polymorphs **1α**, **1β** and **1γ** towards water) is of paramount importance since it has a great impact on bioavailability and storage issues.

List of Schemes.

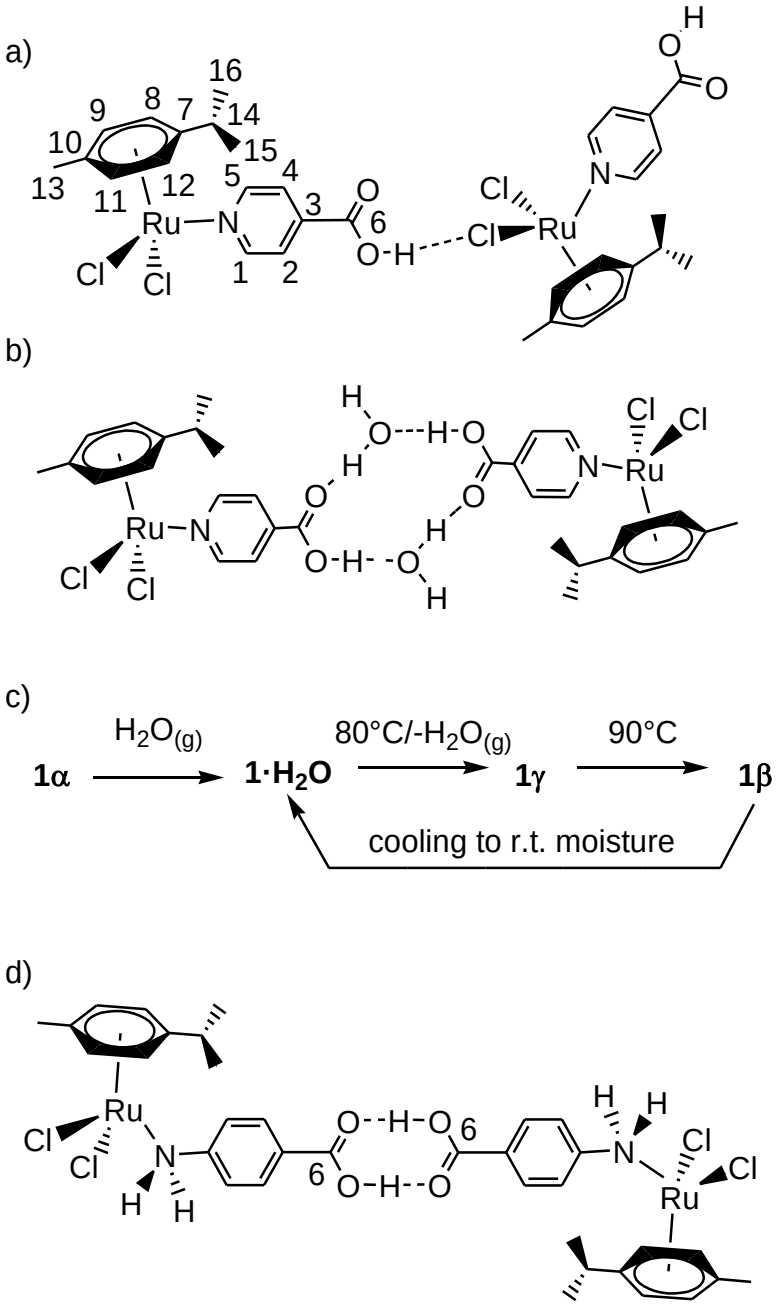

Scheme 1. a) General scheme with atom labeling of **1**, [(p-cymene)Ru(κN-INA)Cl_2], with the hydrogen bonding motif characterizing **1α** and **1β**. b) Hydrogen bonding motif of **1·H_2O**. c) Originally-proposed hydration-dehydration process of complex **1**. General scheme with relevant atom labelling and hydrogen bonding motif of **2**, [(p-cymene)Ru(κN-A4AB)Cl_2].

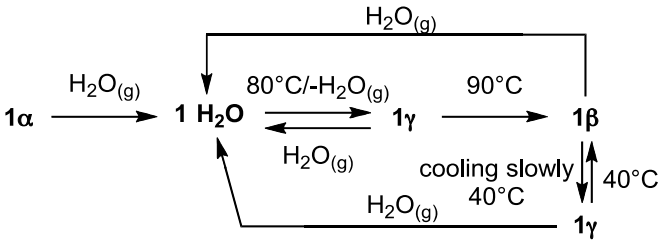

Scheme 2. New hydration-dehydration processes of the complex [(p-cymene)Ru(κN-INA)Cl_2].

List of Figures.

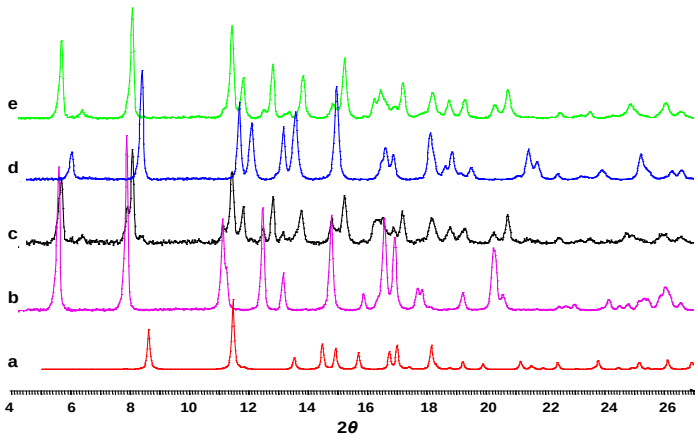

Figure 1. Powder patterns of (a) **1**α, as calculated from the single crystal structure; (b) **1·H$_2$O** at RT; (c) **1**γ, as recorded after 300' annealing at T= 80 °C of **1·H$_2$O**; (d) **1**β at T=373K (e) **1**γ as recorded after cooling at RT, under N_2 atmosphere, of **1**β.

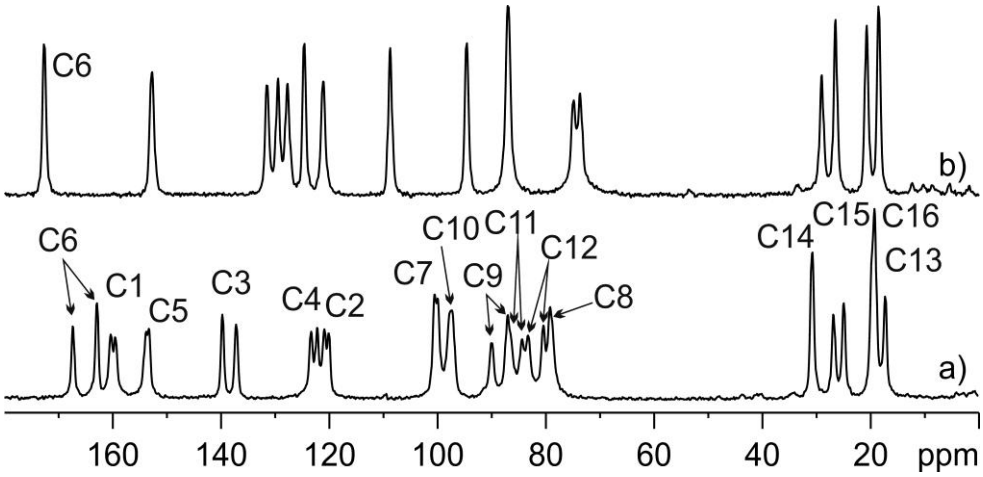

Figure 2. ^{13}C (100.65 MHz) CPMAS spectra with relevant signal assignments of compounds **1γ** (a) and **2** (b) recorded with a spinning speed of 12 kHz.

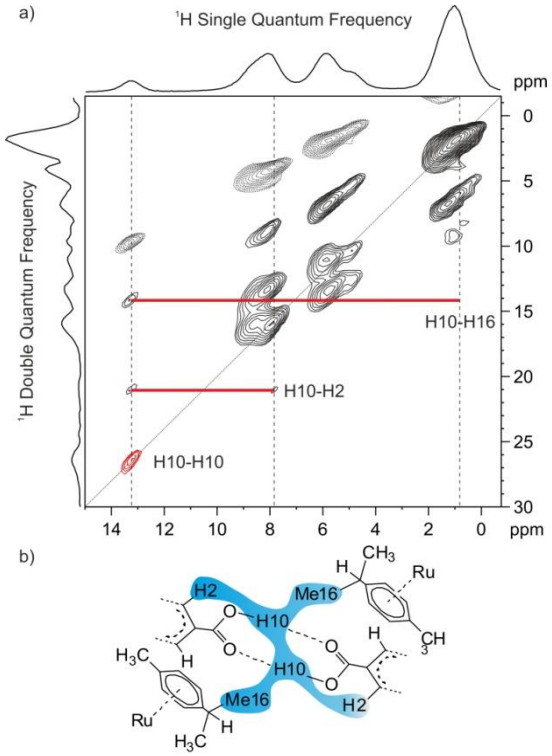

Figure 3. ^{1}H (400.23 MHz) DQ CRAMPS (PMLG5-POSTC7-*w*PMLG5) spectrum of **2** together with skyline projections recorded at 12.5 kHz MAS. Negative contours (artificial peaks) and the F1 = 2F2 diagonal are shown as dashed lines. Solid red horizontal bars indicate specific DQ coherences between OH (H10) and nearby protons. The OH diagonal peak indicating the cyclic dimerization of the COOH groups is highlighted in red. (b) Representation of the crystal structure of **2** showing the intermolecular proximity between H10 and H16 and the intramolecular proximity between H10 and H2.

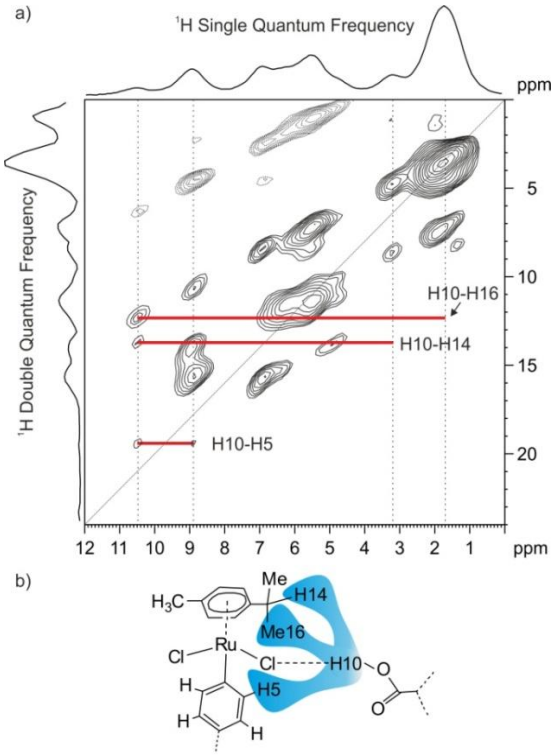

Figure 4. (a) ^{1}H (400.23 MHz) DQ CRAMPS (PMLG5-POSTC7-*w*PMLG5) spectrum of **1γ** together with skyline projections recorded at 12.5 kHz MAS. Negative contours (artificial peaks) and the F1 = 2F2 diagonal are shown as dashed lines. Solid red horizontal bars indicate specific DQ coherences between OH (H10) and nearby protons. (b) Representation of the crystal structure of **1γ** showing H10-H16, H10-H14 and H10-H5 proximities.

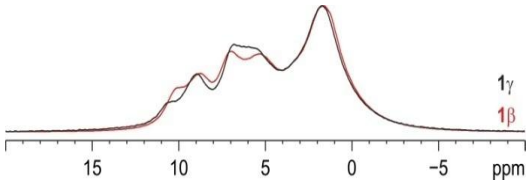

Figure 5. Comparison between ^{1}H (400.23 MHz) MAS spectra of compounds **1β** (red) and **1γ** (black) recorded with a spinning speed of 32 kHz. The technique is quantitative.

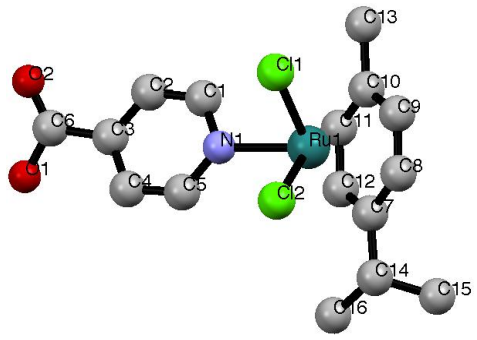

Figure 6. The molecular structure and labeling scheme of **1γ**.

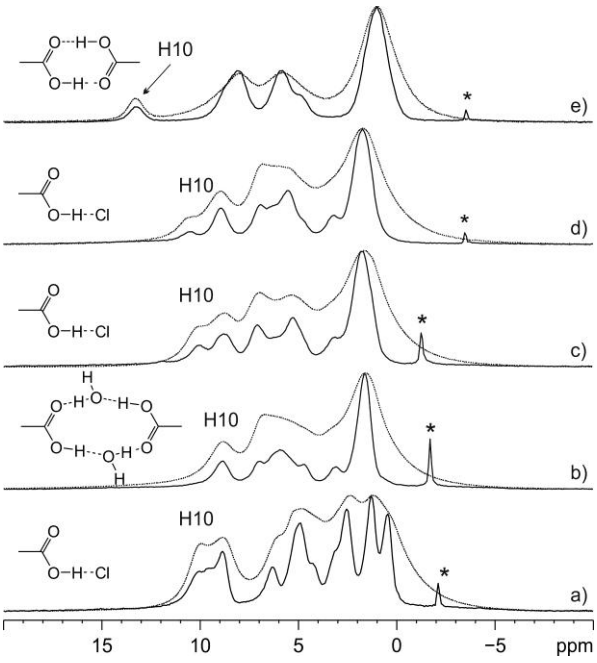

Figure 7. ^{1}H (400.23 MHz) CRAMPS (*w*PMLG5) (black lines) and MAS (grey lines) spectra of compounds **1α** (a), **1·H$_2$O** (b), **1β** (c), **1γ** (d) and **2** (e) recorded with a spinning speed of 12.5 (CRAMPS) and 32 (MAS) kHz. Assignments of hydrogen-bonded proton signals are also reported with hydrogen bonding network schemes. Asterisks denote carrier frequencies.

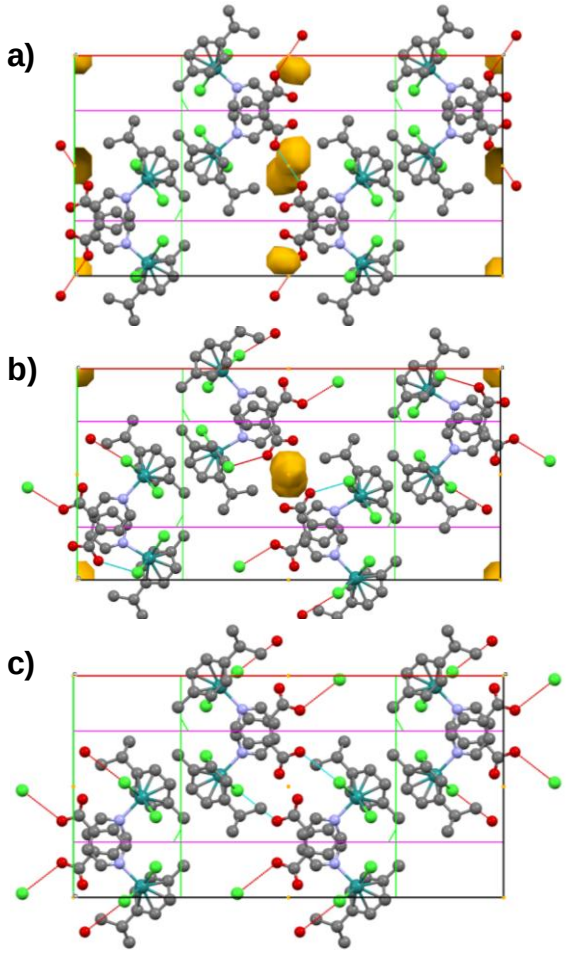

Figure 8. Structure correlation among **1·H$_2$O**, **1γ** and **1β**. All structures have been drawn down their *c* axis and the O-H···Cl interactions highlighted. (a) supercell of **1·H$_2$O**, P2$_1$/a, a = 31.57, b = 15.84, c = 7.42Å, β = 82.25°, V = 3677 Å^3(water molecules have been omitted for clarity but they are located within the volumes highlighted in gold and the carboxylic oxygen atoms mutually interacting through them have been connected by dashed lines); (b) (true) unit cell of **1γ**, P2$_1$/a, a = 30.956, b = 15.358, c = 7.376 Å, β = 95.27°, V = 3492 Å^3; the golden regions are real 'voids' (33 Å^3); (c) supercell of **1β**, P2$_1$/a, a = 29.32, b = 15.089, c = 7.726 Å, β = 97.03°, V = 3389 Å^3.

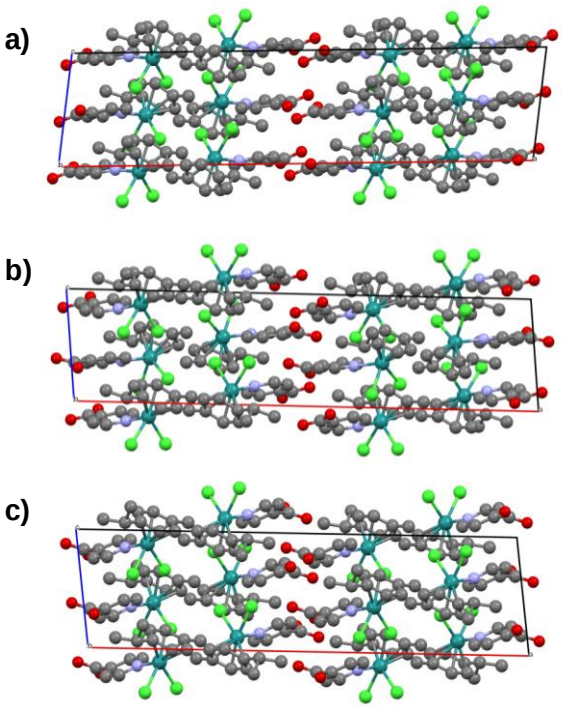

Figure 9. a) supercell of **1·H$_2$O**, b) (true) unit cell of **1γ**and c) supercell of **1β**drawn down their *b* axis.

List of Tables.

Table 1. ^{1}H and ^{13}C chemical shifts (ppm) with assignments for compound **1γ** (for atom labeling see Scheme 1a).

Carbon[a]	**Type**	**^{13}C δ**	**^{1}H δ C-H**
C1	CH	160.3/159.5	9.1 H1
C2	CH	120.8/120.0	7.1 H2
C3	C_q	139.7/137.1	-
C4	CH	123.3/122.2	6.6/6.5 H4
C5	CH	153.8/153.3	8.8/8.9 H5
C6	COOH	167.3/162.9	10.5 H10 OH[a]
C7	C_q	100.5/99.9	-
C8	CH	79.2	5.0 H8
C9	CH	89.9/87.0	5.5/5.5 H9
C10	C_q	97.4	-
C11	CH	86.5sh/84.3	5.6/5.4 H11
C12	CH	83.2/80.5	5.0/5.4 H12
C13	CH_3	19.2/17.3	1.7/1.4 H13
C14	CH	30.8	3.2 H14
C15	CH_3	26.8/24.9	1.8/1.6 H15
C16	CH_3	19.2	1.4 H16

[a] It was not possible to individuate the other OH signal due to overlap with other resonances. Thus, only the OH involved in the strong O-H···Cl HB is reported.

Table 2. ^{1}H DQ correlations[a](in ppm) involving OH ^{1}H Nuclei (<3.0 Å) in **1α**, **1·H$_2$O**, **1β**, **1γ** and **2** (see Fig. 4 and 5, and Fig. S4, S5 and S6 in the supporting information).

Compound	δ_{SQ}	δ_{SQ}	δ_{DQ}	Correlation
1α	9.9	5.0	14.9	H10-H11
1·H$_2$O	8.7	1.4	10.1	H10-H16
	8.7	4.7	13.4	H10-Hw
1β	10.1	1.6	11.7	H10-H16 and H15
	10.1	8.5	18.6	H10-H2
1γ[b]	10.5	1.7	12.2	H10-H16
	10.5	3.2	13.7	H10-H14
	10.5	8.9	19.4	H10-H5
2	13.3	0.9	14.3	H10-H16
	13.3	7.8	21.1	H10-H2[c]
	13.3	13.3	26.6	H10-H10

[a] Only intermolecular proximities are reported. [b] In the unit cell two independent molecules are present. Here only the molecule with the OH proton involved in the strong O-H···Cl HB is considered. [c] intramolecular proximity.

Supporting Information. X-ray crystallographic files in CIF format; crystal data for **1β** and **1γ**; additional schemes and figures. This material is available free of charge via the Internet at http://pubs.acs.org.

Corresponding Authors. angelo.sironi@unimi.it; roberto.gobetto@unito.it

Author Contributions. The manuscript was written through contributions of all authors. All authors have given approval to the final version of the manuscript.

Acknowledgment. We acknowledge financial support from MIUR (PRIN2006 and PRIN2007)

Table of Content Synopsis (TOC)

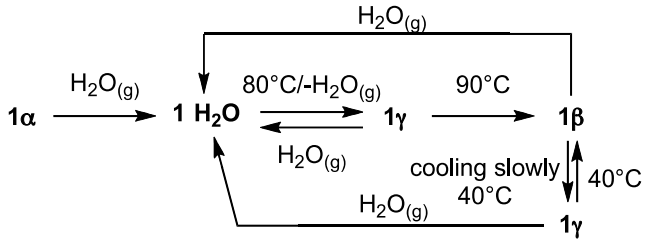

XRPD and SS NMR are complementary techniques providing long and short range information, respectively, which can be further refined by DFT periodic lattice calculations. This combined approach has allowed to shed light on the qualitative phase diagram of the [(*p*-cymene)Ru(κN-INA)Cl_2] (INA = isonicotinic acid) polymorphic system and to fully characterize the changes in the hydrogen bond networks inherent to all these phase transformations.

References and Notes.

[1] (a) Braga, D.; Giaffreda, S.L.; Grepioni, F.; Maini, L.; Polito, M.;*Coord. Chem. Rev.***2006**, *250*, 1267.(b) Lim, G.K.; Fujii, K.; Harris, K.D.M.; Apperley, D.C.; *Cryst. Growth Des.***2011**, *11*, 5192.(c) SLong, S.H.; Parkin, S.; Siegler, M.; Brock, C.P.; Cammers, A.; Li, T.L.; *Cryst. Growth Des.* **2008**, *8*, 3137.

[2] a) Braga, D.; Grepioni, F.; Maini, L.; Prosperi, S.; Gobetto, R.; Chierotti, M. R.; *Chem. Commun.***2010**, *46*, 7715.(b) Lou, B.Y.; Hu, S.L.; *J. Chem. Cryst.***2011**, *41*, 1663.(c) Braga, D.; Dichiarante, E; Palladino, G.; Grepioni, F.; Chierotti, M. R.; Gobetto, R.; Pellegrino, L.; *Cryst. Eng. Comm.***2010**, *12*, 3534.

[3] Masciocchi, N.; Sironi, A.; *Dalton Trans.***1997**, 4643-4650

[4] (a) Tobbens, D.M.; Glinneman, J.; Chierotti, M.R.; van de Streek, J.; Sheptyakov, D.; *Cryst. Eng. Comm.***2012**, *14*, 3046. (b) Schmidt, M.U.; Bruning, J.; Glinnemann, J.; Hutzler, M.W.; Morschel, P.; Ivashevskaya, S.N.; van de Streek, J.; Braga, D.; Maini, L.; Chierotti, M.R.; Gobetto, R.; *Angew. Chem. Int. Ed.***2011**, *50*, 7924.(c) Masciocchi, N.; Galli, S.; Alberti, E.; Sironi, A.; Di Nicola, C.; Pettinari, C.; Pandolfo, L.;*Inorg. Chem.***2006**, *45*, 9064.

[5] (a) Bradley, J.P.; Velaga, S.P.; Antzutkin, O.N.; Brown, S.P.;*Cryst. Growth Des.***2011**, *11*, 3463.(b) Bettini, R.; Menabeni, R.; Tozzi, R.; Pranzo, M. B.; Pasquali, I.; Chierotti, M. R.; Gobetto, R.; Pellegrino, L.;*J. Pharm. Sci.***2010**, *99*, 1855.

[6] (a) Lesage, A.; Sakellariou, D.; Hediger, S.; Elena, B.; Charmont, P.; Steuernagel, S.; Emsley, L.;*J.Magn. Reson.***2003**, *163*, 105. (b) EVinogradov E.; Madhu P.K.; Vega S.;*Chem. Phys. Lett.***2002**, *354*, 193.(c) Schnell, I.; Spiess, H.W.;*J. Magn. Reson.***2001**, *151*, 153.

[7] (a) Chierotti, M. R.;Gobetto, R. in *Supramolecular Chemistry: From Molecules to Nanomaterials* (Eds. P.A. Gale, J.W. Steed), John Wiley & Sons, Ltd., 2012, pp. 331-345; (b) Chierotti, M. R.;Gobetto, R.;*Chem. Commun.***2008**, 1621.

[8] (a) Beko, S.L.; Thoms, S.D.; Bruning, J.; Alig, E.; van de Streek, J.; Lakatos, A.; Glaubitz, C.; Schmidt, M.U.;*Z. Kristallogr.***2010**, *225*, 382.(b) Bradley, J.P.; Pickard, C.J.; Burley, J.C.; Martin, D.R.; Hughes, L.P.; Cosgrove, S.D.; Brown, S.P.; *J. Pharm. Sci.* **2012**, *101*, 1821.

[9] Bacchi, A.; Cantoni, G.; Chierotti, M. R.; Girlando, A.; Gobetto, R.; Lapadula, G.; Pelagatti, P.; Sironi, A.; Zecchini, M.; *CrystEngComm.***2011**, *13*, 4365.

[10] (a) Soldatov, D. V. *J. Chem. Crystallogr*. **2006**, *36*, 747-768. (b) Bacchi, A.; Cantoni, G.; Pelagatti, P.; Rizzato, S. *J. Organomet. Chem.***2012**, *714*, 81-87.

[11] Bacchi, A.; Carcelli, M.; Pelagatti, P. *Crystallogr. Rev.***2012**, *18*, 253-279.

[12] (a) Braga, D.; Grepioni, F. *Chem. Soc. Rev*. **2000**, *29*, 229-238. (b) Kumalah, S. A.; Holman, K. T. *Inorg. Chem.* **2009**, *48*, 6860-6872.

[13] Bacchi, A.; Cantoni, G.; Granelli, M.; Mazza, S.; Pelagatti, P; Rispoli, G.;*Cryst. Growth Des.***2011**, *11*, 5039-5047.

[14] vanRossum, B.-J.; de Groot, C. P.;Ladizhansky,V.; Vega, S.; d. Groot,H. J. M.*J. Am. Chem. Soc.* **2000**, *122*, 3465.

[15] Bettini, R.; Menabeni, R.; Tozzi, R.; Pranzo, M.B.; Pasquali,I.; Chierotti,M.R.; Gobetto, R.; Pellegrino, L. *J. Pharm. Sci.***2010**, *99*, 1855.

[16] Vinogradov,E.; Madhu, P. K. ; Vega,S.; *Chem. Phys. Lett.***1999**, *314*, 443.

[17] Hohwy, M.;Jakobsen,H. J.;Edén, M.;Levitt,M. H.; Nielsen, N. C.;*J. Chem. Phys.***1998**, *108*, 2686.

[18] Coelho, A. A.;*J. Appl. Cryst.* **2003**, *36*, 86.

[19] Coelho, A. A.;*J. Appl. Cryst.***2000**, *33*, 899.

[20] We wrote a simple program able to build the plenty of individual-atom to individual-atom penalties necessary to drive the conformational search toward reasonable results.

[21] Cheary, R. W.; Coelho, A.;*J. Appl. Cryst.* **1992**, *25*, 109.

[22] Topas: General profile and structure analysis software for powder diffraction data;*Bruker AXS*, Karlsruhe, Germany, **2001**.

[23] Giannozzi, P.; Baroni, S.; Bonini, N.; Calandra, M.; Car, R.; Cavazzoni, C.; Ceresoli, D.; Chiarotti, G. L.; Cococcioni, M.; Dabo, I.; Dal Corso, A.; de Gironcoli, S.; Fabris, S.; Fratesi, G.; Gebauer, R.; Gerstmann, U.; Gougoussis, C.; Kokalj, A.; Lazzeri, M.; Martin-Samos, L.; Marzari, N.; Mauri, F.; Mazzarello, R.; Paolini, S.; Pasquarello, A.; Paulatto, L.; Sbraccia, C.; Scandolo, S.; Sclauzero, G.; Seitsonen, A. P.; Smogunov, A.; Umari, P.; Wentzcovitch, R. M. *J. Phys.: Condens.Matter***2009**, *21*, 395502.

[24] Vanderbilt, D. *Phys. Rev. B* **1990**, *41*, 7892.

[25] http://www.quantum-espresso.org/?page_id=190

[26] Perdew, J. P.; Burke, K; Ernzerhof, M.*Phys. Rev. Lett.* **1996**, *77*,3865.

[27] Monkhorst, H. J.; Pack, J. D.*Phys.Rev. B***1976**, *13*, 5188.

[28] Gaussian 09, Revision C.01, Frisch, M. J.; Trucks, G. W.; Schlegel, H. B.; Scuseria, G. E.; Robb, M. A.; Cheeseman, J. R.; Scalmani, G.; Barone, V.; Mennucci, B.; Petersson, G. A.;

Nakatsuji, H.; Caricato, M.; Li, X.; Hratchian, H. P.; Izmaylov, A. F.; Bloino, J.; Zheng, G.; Sonnenberg, J. L.; Hada, M.; Ehara, M.; Toyota, K.; Fukuda, R.; Hasegawa, J.; Ishida, M.; Nakajima, T.; Honda, Y.; Kitao, O.; Nakai, H.; Vreven, T.; Montgomery, Jr., J. A.; Peralta, J. E.; Ogliaro, F.; Bearpark, M.; Heyd, J. J.; Brothers, E.; Kudin, K. N.; Staroverov, V. N.; Kobayashi, R.; Normand, J.; Raghavachari, K.; Rendell, A.; Burant, J. C.; Iyengar, S. S.; Tomasi, J.; Cossi, M.; Rega, N.; Millam, J. M.; Klene, M.; Knox, J. E.; Cross, J. B.; Bakken, V.; Adamo, C.; Jaramillo, J.; Gomperts, R.; Stratmann, R. E.; Yazyev, O.; Austin, A. J.; Cammi, R.; Pomelli, C.; Ochterski, J. W.; Martin, R. L.; Morokuma, K.; Zakrzewski, V. G.; Voth, G. A.; Salvador, P.; Dannenberg, J. J.; Dapprich, S.; Daniels, A. D.; Farkas, Ö.; Foresman, J. B.; Ortiz, J. V.; Cioslowski, J.; Fox, D. J. Gaussian, Inc., Wallingford CT, **2009**.

[29] Becke, A. D. J. *Chem. Phys.***1993**, *98*, 5648.

[30] Lee, C.; Yang, W.; Parr, R. G.*Phys. Rev. B: Condens. Matter***1988**, *37*, 785.

[31] Brown, S. P.; Xia Zhu,X.;Saalwalchter, K.;Spiess, H. W. *J. Am. Chem. Soc.* **2001**, *123*, 4275.

[32] In practice, this was done by finding the best description of the **1γ**-DFT model with the rigid groups used in the XRPD analysis by an 'only penalties' simulated annealing approach; and, subsequently, by optimizing the **1γ**-XRPD model freeing the rigid body translations but imposing that the refined torsional and rotational degrees of freedom, described in the experimental section, where within the range of 2° of those describing **1γ**-DFT.

[33] Pickard,C. J.;Mauri, F. *Phys. Rev. B* **2001**, *63*, 245101.

[34] Semi-quantitatively analysis done by comparing the absolute energy per molecule of the two cells since **1γ** contains exactly twice the atoms of **1β**.

[35] (a) Brammer, L.; Bruton, E. A.; Sherwood, P. *Cryst. Growth Des.***2001**, *1*, 277-290. (b) Brammer, L. *Dalton Trans.***2003**, 3145-3157.

[36] Etter, M. C. *Acc. Chem. Res.***1990**, *23*, 120.

[37] Note that A4AB is known to exist in two polymorphs: α and β. (a) Athimoolam, S.; Natarajan, S. *Acta Cryst.***2007**, *C63*, o514-o517. (b) Gracina, S.; Fischer, A.*Acta Cryst.***2005**, *E61,* o1242-o1244. Only the α form presents the supramolecular carboxylic group dimerization. Thus, in this article we refer to this form only.

[38] Takusagawa, F.; Shimeda, A. *Acta Crystallogr. Sect. B: Struct. Crystallogr. Cryst. Chem.***1976**, *32*, 1925.

[39] (a) Liu, H.-K.; Sadler, P. J. *Acc. Chem. Res.***2011**, *44*, 349-359. (b) Wang, F.; Abtemariam, A.; van der Geer, E. P. L.; Fernández, R.; Melchart, M.; Deeth, R. J.; Aird, R.; Guichard, S.; Fabbiani, F. P. A.; Lozano-Casal, P.; Oswald, I. D. H.; Jodrell, I. D.; Parsons, S.; Sadler, P. J. *PNAS***2005**, *102*, 18269-18274.

Electronic Supplementary Information (ESI)

For

Probing hydrogen bond networks in half-sandwich Ru(II) building-blocks by a combined 1H DQ CRAMPS solid-state NMR, XRPD and DFT approach

Michele R. Chierotti,[a] *Roberto Gobetto,*[a]* *Carlo Nervi,*[a] *Alessia Bacchi,*[b] *Paolo Pelagatti,*[b] *Valentina Colombo,*[c] *Angelo Sironi* [c]*

[a]Department of Chemistry and NIS Centre of Excellence, University of Torino, Via P. Giuria 7, 10125 Torino, Italy.

[b] Department of Chemistry, University of Parma, Parco Area Scienze 17/A, 43124 Parma, Italy.

[c] Department of Chemistry, University of Milano, Via Golgi 19, 20133 Milano, Italy.

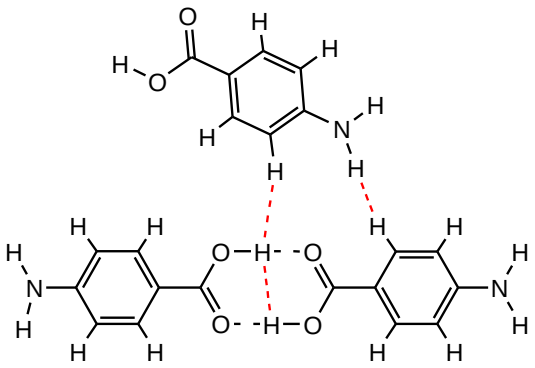

Scheme S1 Crystal packing of A4AB with the supramolecular cyclic dimerization of the carboxylic groups. ^{1}H-^{1}H proximities observed in the ^{1}H DQ CRAMPS spectrum are highlighted in red.

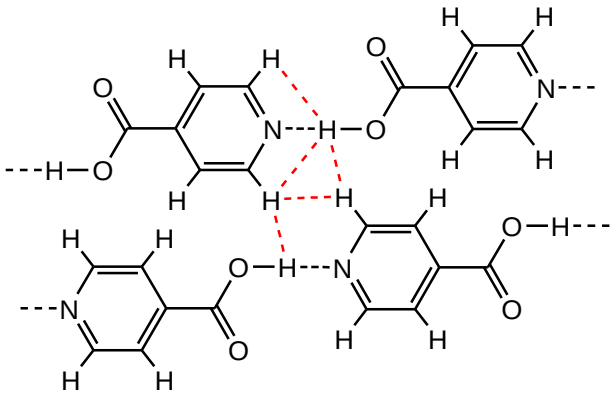

Scheme S2. Crystal packing of INA with the head-to-tail HB arrangement. ^{1}H-^{1}H proximities observed in the ^{1}H DQ CRAMPS spectrum are highlighted in red.

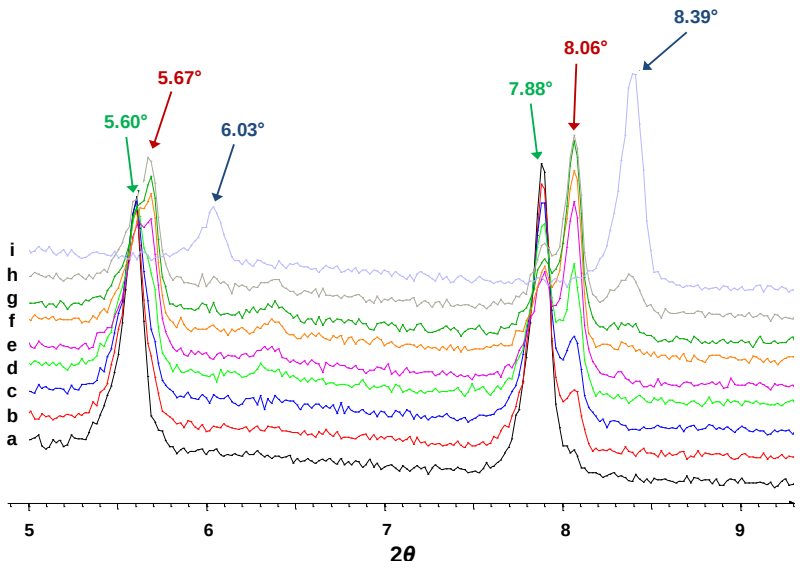

Fig S1. XRPD monitoring of the dehydration process of **1·H_2O** at 80°C. Powder patterns recorded at (a) t=0' (this powder pattern is analogous to that one recorded at room temperature), (b) t=30', (c) t=60', (d) t=180', (e) t=210', (f) t=270', (g) t=300', (h) t=360', and (i) t=1260'. Coloured arrows indicate peak maxima of **1·H_2O** (green), **1β** (blue), and **1γ** (red) phases.

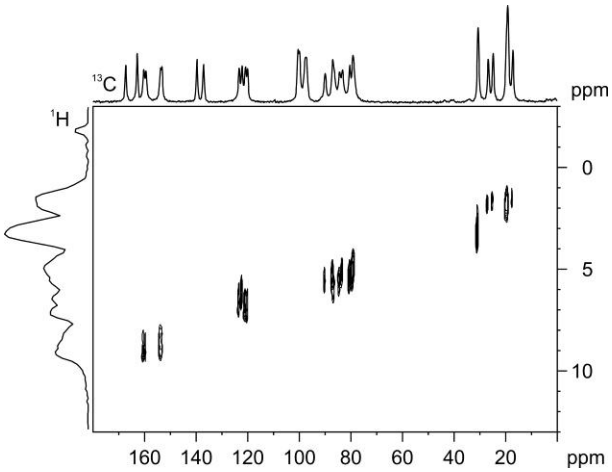

Fig. S2. ^{1}H-^{13}C FSLG-HETCOR spectrum of **1γ** recorded with a spinning speed of 12 kHz and a contact time of 100 μs.

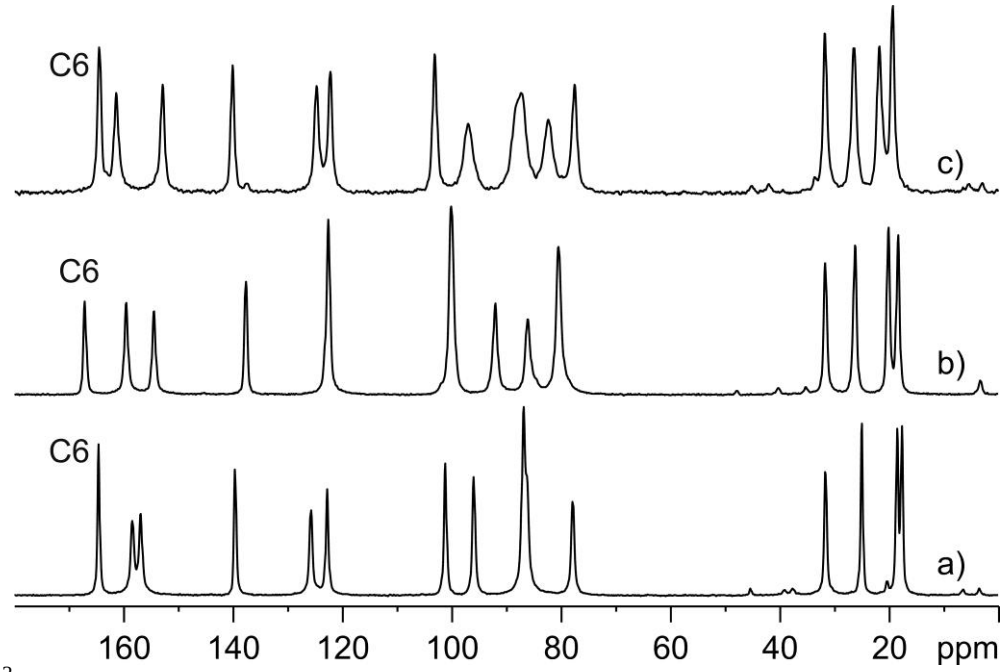

Fig. S3. ^{13}C (100.65 MHz) CPMAS spectra with relevant assignments of compounds **1α** (a), **1·H$_2$O** (b), and **1β**(c) recorded with a spinning speed of 12 kHz. Adapted from ref 9 by permission of The Royal Society of Chemistry.

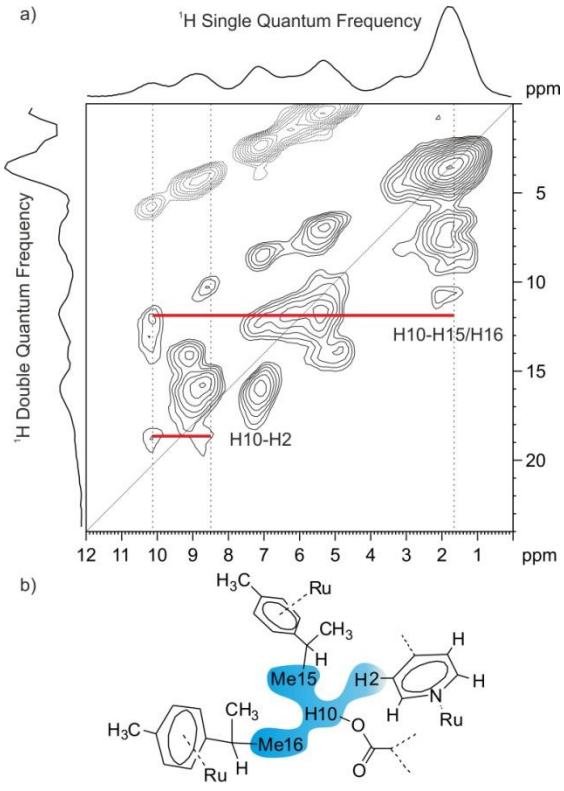

Fig. S4. (a) ^{1}H (400.23 MHz) DQ CRAMPS spectrum of **1β** together with skyline projections recorded at 12.5 kHz MAS. Negative contours (artificial peaks) and the F1 = 2F2 diagonal are shown as dashed lines. Solid red horizontal bars indicate specific DQ coherences between OH (H10) and nearby protons. (b) Representation of the crystal structure of **1β** showing OH-H15, OH-H16 and OH-H2 proximities.

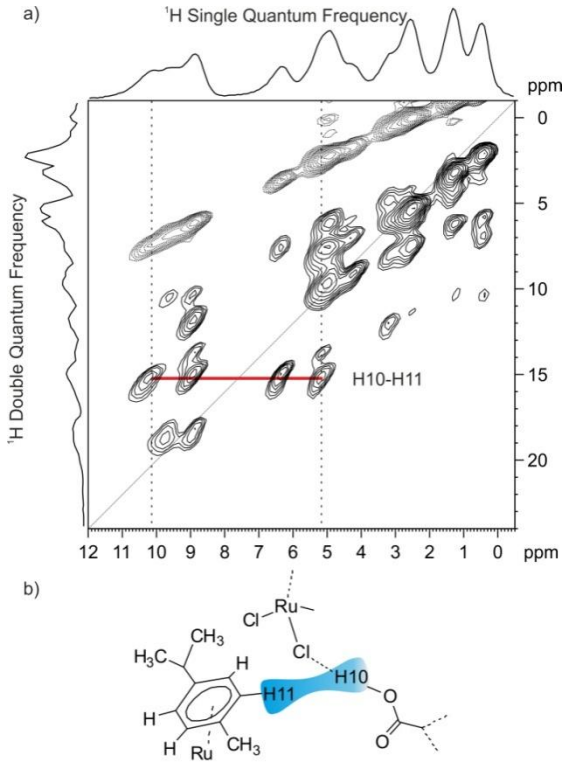

Fig. S5. (a) ^{1}H (400.23 MHz) DQ CRAMPS spectrum of **1α** together with skyline projections recorded at 12.5 kHz MAS. Negative contours (artificial peaks) and the F1 = 2F2 diagonal are shown as dashed lines. Solid red horizontal bars indicate specific DQ coherences between OH (H10) and nearby protons. (b) Representation of the crystal structure of **1α** showing the proximity between OH and the aromatic proton H11.

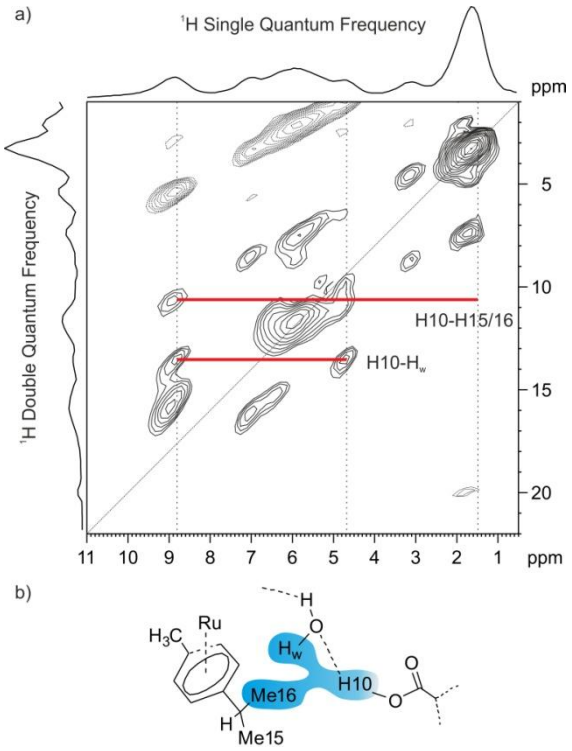

Fig. S6. (a) ^{1}H (400.23 MHz) DQ CRAMPS spectrum of **1·H$_2$O** together with skyline projections recorded at 12.5 kHz MAS. Negative contours (artificial peaks) and the F1 = 2F2 diagonal are shown as dashed lines. Solid red horizontal bars indicate specific DQ coherences between OH (H10) and nearby protons. Other DQ signals around 16-17 ppm refer to proximities of H1 (8.6 ppm) and H5 (8.9 ppm) with other nuclei. (b) Representation of the crystal structure of **1·H$_2$O** showing the proximity between OH and the water molecule proton and between OH-H16 and H15.

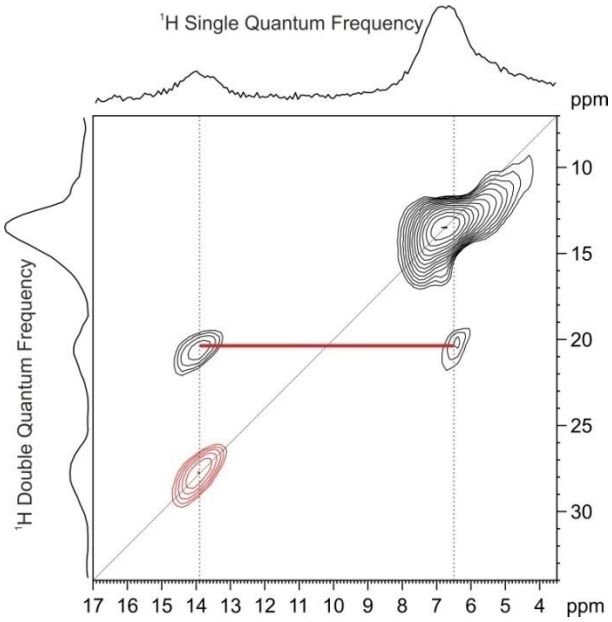

Fig. S7. ^{1}H (400.23 MHz) DQ CRAMPS spectrum of A4AB together with skyline projections recorded at 12.5 kHz MAS. The F1 = 2F2 diagonal is shown as dashed lines. Solid red horizontal bars indicate specific DQ coherences between OH (H10) and nearby protons while OH diagonal peak indicating the cyclic dimerization of the COOH groups is highlighted in red. DQ signals are observed at δ_{DQ}=13.9+13.9=27.8 (OH-OH diagonal peak), δ_{DQ}=13.9+6.6=20.5 (OH-H3 and NH) and δ_{DQ}=6.7+6.7=13.4 (H2-H3, H5-H6 and NH-NH and NH-aromatic protons).

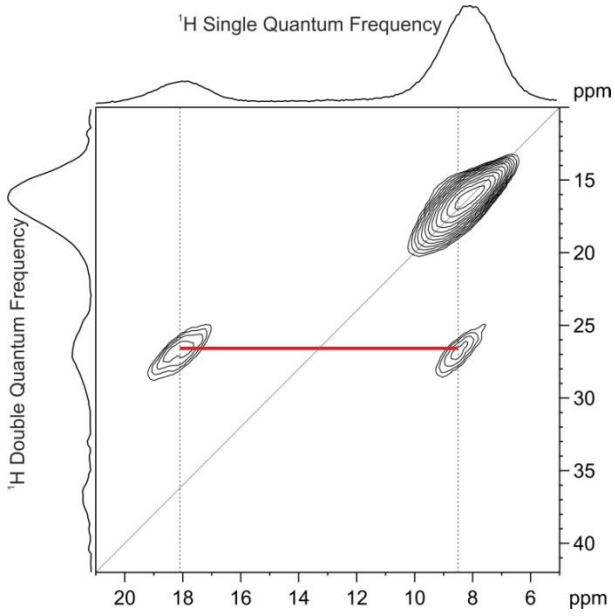

Fig. S8. ^{1}H (400.23 MHz) DQ CRAMPS spectrum of INA together with skyline projections recorded at 12.5 kHz MAS. The F1 = 2F2 diagonal is shown as dashed lines. Solid red horizontal bars indicate specific DQ coherences between OH (H10) and nearby protons. DQ signals are observed at δ_{DQ}=18.1+8.5=26.6 (OH-H2 and H6 pyridine hydrogen atoms) and δ_{DQ}=8.2+8.2=16.4 (H2-H3 and H5-H6 pyridine hydrogen atoms).

X-ray powder diffraction measurements and analysis. All the diffraction data (Cu Kα, 1.5418 Å) were collected on a θ:θ Bruker Axs D8 Advance vertical scan diffractometer; the generator was operated at 40 kV and 40 mA. The diffractometer was equipped with a Ni filter and a linear Position Sensitive Detector (PSD), with the following optics: primary and secondary Soller slits, 2.3 and 2.5°, respectively; divergence slit, 0.3°; receiving slit, 8 mm. The nominal resolution for the present set-up is 0.08° 2θ (FWHM of the α1 component) for the LaB_6 peak at about 21.3° (2θ). The conditioning chamber for thermodiffractometric experiment, a closed Peltier sample heater, was supplied by Officina Elettrotecnica di Tenno, Italy. The accurate diffraction pattern at RT under nitrogen of the pure **1γ** phase was acquired in the 4-90° 2θ range, with Δ2θ = 0.02° and exposure time 1 s/step. Indexing was performed with the aid of the single value decomposition approach,[i] as implemented in the TOPAS-R suite of programs.[ii] Even if the presence of two independent molecules in the asymmetric unit was immediately recognized from the proposed cell volumes, the actual determination of the correct cell parameters was quite hard since it was not clear if two peaks, at ca. 13.4° and 26°, were due to an impurity or not. Depending on this choice, we obtained two classes of lattices with different molecular volumes ($V_M = V/Z$): either ca 400 or 435 $Å^3$. The former value sounded better being similar to that of **1β**. However, exhaustive simulated-annealing runs[iii] failed to afford a reasonable structural solution (both for triclinic and monoclinic cells). Accordingly, we analysed the cells with larger molecular volumes and we selected the best candidate (P21/c, a = 30.96, b = 15.37, c = 7.39, β = 95.22; Rwp 4.55) on the base of Le Bail refinements, in the 4-47° 2θ region, (one of the other alternatives being: P21/c, a =7.39, b = 30.82, c = 15.53, β = 98.29; Rwp = 5.01). Exhaustive simulated-annealing runs afforded a potentially reasonable structural solution with a Rwp of 13.21 which however was still considered with suspect due to the "anomalous" molecular

volume. Eventually, while simulated-annealing was still crunching numbers in P21/c, after reconsidering the whole indexing results, we realized that a Le Bail refinement in P21/a was leading to an even better Rwp (P21/a, a = 30.986(2), b = 15.3681(9), c = 7.3828(4), β = 95.281(4); Rwp 4.39). Later on, a simulated-annealing solution with a Rwp of 10.15 was obtained in the new space group. During simulated annealing, we described the molecule as a single "flexible" rigid body allowing for all necessary rotations. At variance, during refinements, the Ru-(η^6-p-cimene) and the p-carboxyl pyrimidine groups were treated as independent, "flexible" (the isopropyl and carboxyl group rotations were allowed, respectively) rigid bodies. The chlorine atoms were free to refine but the Ru-Cl and Ru-N bond distances were restrained to 2.44 and 2.12 Å, respectively. "Antibump" conditions were substantial for a correct sampling of the conformational space and we wrote a simple program able to build the plenty of individual-atom to individual-atom penalties necessary to drive the conformational search toward reasonable results. The final refinement was done using the DFT optimized structure as 'reference' maintaining only the Ru-Cl and Ru-N restrans.[iv]

Peak shapes were described by the fundamental parameters approach.[v] The experimental background was fit by a polynomial description. Systematic errors were modelled with sample-displacement angular shifts corrections. Metal and chlorine atoms were given a refinable, isotropic displacement parameter (BM) while lighter atoms were assigned a common B = BM + 2.0 $Å^2$ value. Scattering factors, corrected for real and imaginary anomalous dispersion terms, were taken from the internal library of TOPAS. Final Rp, Rwp, RBragg are respectively 4.02, 5.28 and 2.27.

CCDC 944184-944185 contain the supplementary crystallographic data for this paper. These data can be obtained free of charge from The Cambridge Crystallographic Data Centre via www.ccdc.cam.ac.uk/data_request/cif.

Crystal data for 1γ: $C_{32}H_{38}Cl_4N_2O_4Ru_2$, fw = 858.58 g mol^{-1}, monoclinic $P2_1/a$ (No 14, non standard setting of $P2_1/c$), a = 30.915(2), b = 15.3400(9), c = 7.3675(4), β = 95.274(5)°, V = 3479.3(3) Å^3, Z = 8, ρ_{calc} = 1.64 g cm^{-3}, μ(Cu-Kα) = 25.41 cm^{-1}. R_p and R_{wp} = 4.02 and 5.28, respectively, for 4301 data collected in the 4-90° 2θ range. R_{Bragg} = 2.27.

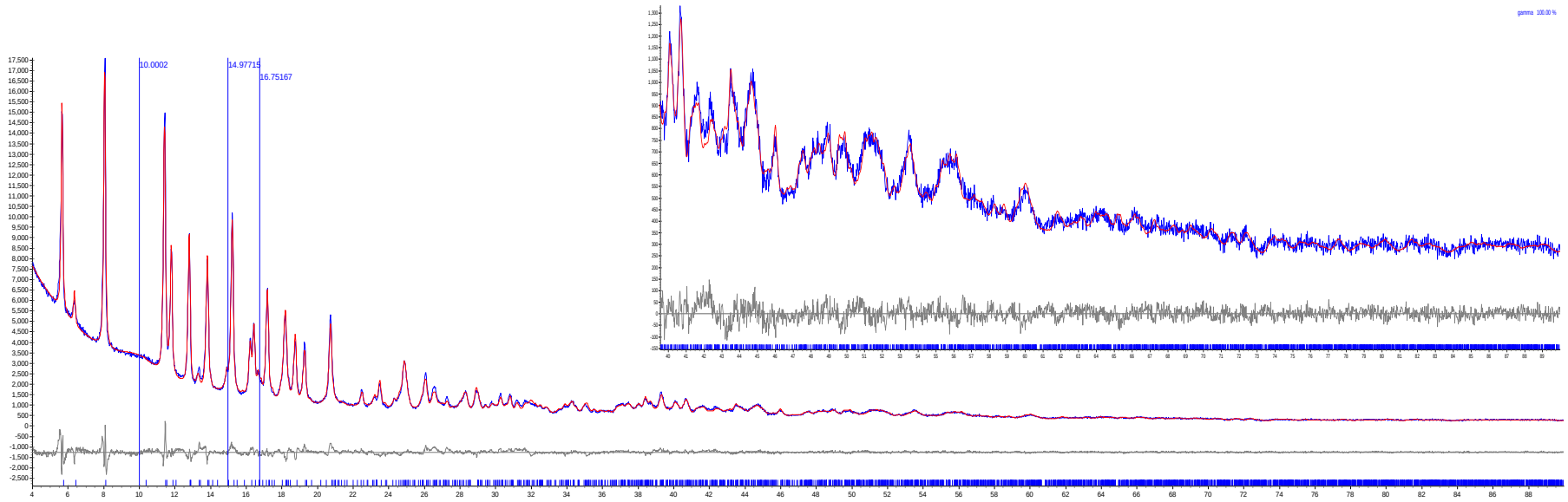

Fig. S9. Rietveld refinement results for **1γ** (final Rp, Rwp, RBragg are respectively 4.02, 5.28 and 2.27) in terms of calculated (red), acquired (blue) and difference (grey) diffractograms. Peak markers are depicted at the bottom. Horizontal axis = 2θ, °; vertical axis = intensity, counts. For the sake of clarity, the portion above 40° has been magnified in the inset. The bump at about 10° is due to the sample-holder while the peaks at 14.98 ° and 16.75 belong to traces of **1·H$_2$O**.

Crystal data for 1β: $C_{16}H_{19}Cl_2NO_2Ru$, fw = 429.29 g mol^{-1}, monoclinic $P2_1/a$ (No 14, non standard setting of $P2_1/c$), a = 14.705(1), b = 15.086(1), c = 7.7234(5), β = 98.045(4)°, V = 1696.5(2) $Å^3$, Z = 4, ρ_{calc} = 1.68 g cm^{-3}, μ(Cu-Kα) = 26.06 cm^{-1}. R_p and R_{wp} = 4.89 and 6.52, respectively, for 4301 data collected in the 4-90° 2θ range. R_{Bragg} = 3.00.

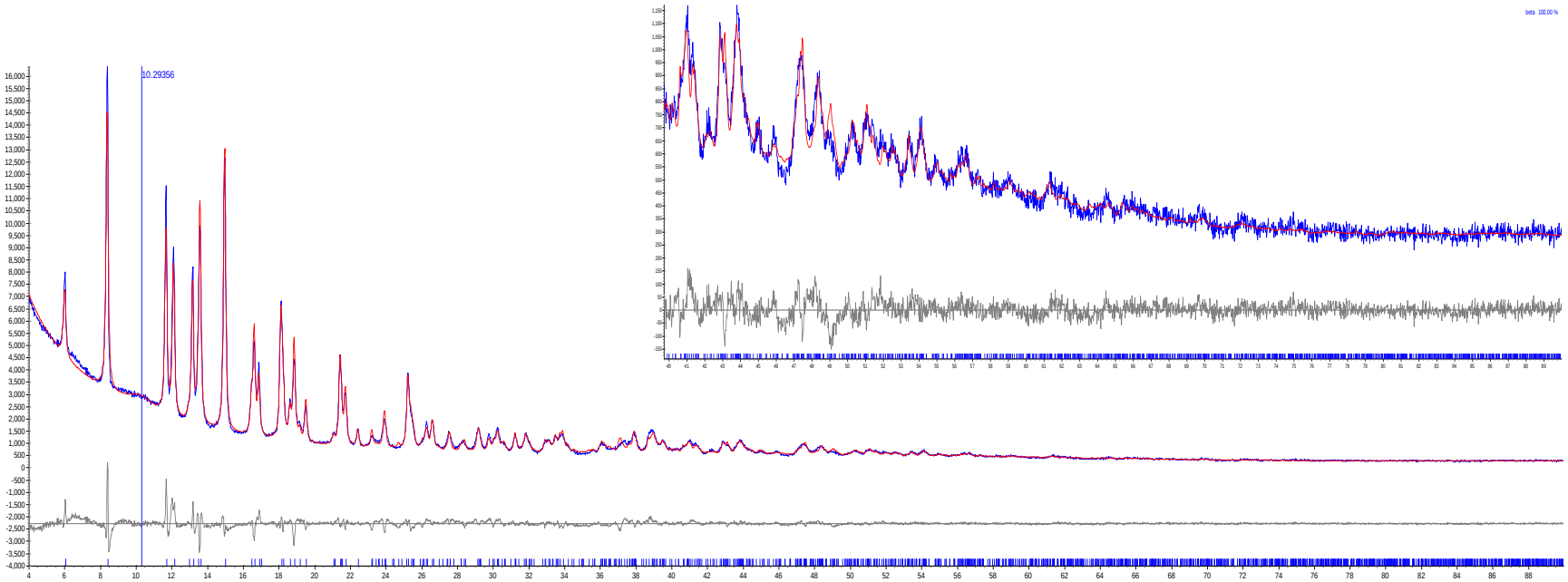

Fig. S10. Rietveld refinement results for **1β** (final Rp, Rwp, RBragg are respectively 4.89, 6.52 and 3.00) in terms of calculated (red), acquired (blue) and difference (grey) diffractograms. Peak markers are depicted at the bottom. Horizontal axis = 2θ, °; vertical axis = intensity, counts. For the sake of clarity, the portion above 40° has been magnified in the inset. The bump at about 10.3° is due to the sample-holder.

[i] Coelho, A. A.;*J. Appl. Cryst.***2003**, *36*, 86.

[ii] Topas-R: General profile and structure analysis software for powder diffraction data;*Bruker AXS*, Karlsruhe, Germany, **2001**.

[iii] Coelho, A. A.;*J. Appl. Cryst.***2000**, *33*, 899.

[iv] In practice, this was done by finding the best description of the **1γ**-DFT model with the rigid groups used in the XRPD analysis by an 'only penalties' simulated annealing approach; and, subsequently, by optimizing the **1γ**-XRPD model freeing the rigid body translations but imposing that the refined torsional and rotational degrees of freedom, described in the experimental section, where within the range of 2° of those describing **1γ**-DFT.

[v] Cheary, R. W.; Coelho, A.;*J. Appl. Cryst.***1992**, *25*, 109.